IRMPD Spectroscopy of Anionic Group II Metal Nitrate Cluster Ions

Christopher M. Leavitt,[a] Jos Oomens,[b] Ryan P. Dain,[a] Jeffrey Steill,[b] Gary S. Groenewold,[c] and Michael J. Van Stipdonk[a]

[a] Department of Chemistry, Wichita State University, Wichita, Kansas, USA
[b] FOM Institute for Plasma Physics Rijnhuizen, Nieuwegein, The Netherlands
[c] Idaho National Laboratory, Idaho Falls, Idaho, USA

Anionic group II metal nitrate clusters of the formula $[M_2(NO_3)_5]^-$, where M_2 = Mg_2, MgCa, Ca_2, and Sr_2, are investigated by infrared multiple photon dissociation (IRMPD) spectroscopy to obtain vibrational spectra in the mid-IR region. The IR spectra are dominated by the symmetric and the antisymmetric nitrate stretches, with the latter split into high and low-frequency components due to the distortion of nitrate anion symmetry by interactions with the cation. Density functional theory (DFT) is used to predict geometries and vibrational spectra for comparison to the experimental spectra. Calculations yield two stable isomers: the first one contains two terminal nitrate anions on each cation and a single bridging nitrate ("mono-bridging"), while the second structure features a single terminal nitrate on each cation with three bridging nitrate ligands ("tri-bridging"). The tri-bridging isomer is calculated to be lower in energy than the mono-bridging one for all species. Theoretical spectra of the tri-bridging structure provide a better qualitative match to the experimental infrared spectra of $[Mg_2(NO_3)_5]^-$ and $[MgCa(NO_3)_5]^-$. However, the profile of the low-frequency ν_3 band for the Mg_2 complex suggests a third possible isomer not predicted by theory. The IRMPD spectra of the Ca_2 and Sr_2 complexes are better reconciled by a weighted summation of the spectra of both isomers suggesting that a mixture of structures is present. (J Am Soc Mass Spectrom 2009, 20, 772–782) © 2009 Published by Elsevier Inc. on behalf of American Society for Mass Spectrometry

The combination of ion-trapping mass spectrometers and free-electron lasers tunable through the mid-infrared region of the electromagnetic spectrum have provided invaluable access to the vibrational spectra of discrete, gas-phase metal complexes [1–10]. It is generally difficult to acquire a conventional linear absorption spectrum of species commonly investigated by mass spectrometry because of the low ion concentrations. However, use of an action spectroscopy approach allows photon absorption to be monitored by measuring fragmentation yields that result from wavelength-specific infrared multiple-photon dissociation (IRMPD) [11–13].

Using the uranyl (UO_2^{2+}) and the europium (Eu^{3+}) cations, our group produced the first vibrational spectra of gas-phase metal nitrate anions of the formula $[UO_2(NO_3)_3]^-$ and $[Eu(NO_3)_4]^-$ [14]. These experiments were carried out at the FOM Institute for Plasma Physics in Nieuwegein, The Netherlands, using the free electron laser for infrared experiments (FELIX). FELIX provides a tunable, high-intensity beam of photons across the mid-IR range to a high-resolution mass spectrometer. The IRMPD spectra of both the uranyl and europium nitrate anions are dominated by the antisymmetric nitrate stretch (ν_3), which is split into low and high-frequency components corresponding to the O-N-O (O-atoms involved in bonding with the metal), and (non-coordinating) N=O stretches respectively. Previous studies have shown that the splitting of the ν_3 ($\Delta\nu_3$) is proportional to the interaction strength between the metal and the nitrate ligands [15, 16]. In the uranyl and europium nitrate anions, $\Delta\nu_3$ was found to be 264 cm^{-1} and 273 cm^{-1} respectively [14].

In a later study, IRMPD spectroscopy was used to record vibrational spectra of anionic group II metal nitrate complexes of the formula $[M(NO_3)_3]^-$ where M = Mg^{2+}, Ca^{2+}, Sr^{2+}, and Ba^{2+} [17]. By observing differences in the magnitude of $\Delta\nu_3$, it was possible to correlate the polarizing power to the bond strength between the cation and the nitrate ligands. In the IRMPD spectra of the group II trinitrato anions, the high-frequency ν_3 component shifts to the red for metals with a larger radius, while the low-frequency component remains unperturbed irrespective of the metal ion, and $\Delta\nu_3$ values are 231, 229, 218, and 208 cm^{-1} for Mg^{2+}, Ca^{2+}, Sr^{2+}, and Ba^{2+} respectively. A similar trend is observed for the $\Delta\nu_3$ values in the DFT calcu-

Address reprint requests to Dr. M. J. Van Stipdonk, Department of Chemistry, Wichita State University, Wichita, KS 67260-0051, USA. E-mail: mike.vanstipdonk@wichita.edu; Dr. J. Oomens, FOM Institute for Plasma Physics Rijnhuizen, Nieuwegein, The Netherlands; and Dr. G. S. Groenewold, Idaho National Laboratory, Idaho Falls, ID, USA.

Portions of this work were presented at the 56th ASMS Conference on Mass Spectrometry and Allied Topics, Denver CO, June 1–6, 2008.

1044-0305/09/$32.00
doi:10.1016/j.jasms.2008.12.023

Published online January 9, 2009
Received July 17, 2008
Revised December 10, 2008
Accepted December 18, 2008

lations, which shows that the interaction between the metal and nitrate is largest for the magnesium complex and decreases as Mg > Ca > Sr > Ba. DFT calculations of complexes of the formula, $[M(NO_3)]^+$, $[M(NO_3)_2]^0$, and $[M(NO_3)_3]^-$, show that the $\Delta\nu_3$ shift increases as the number of nitrate ligands decreases. In a general comparison with other metal nitrate species, the interaction between group II metals and nitrate is stronger than that between group I metals and nitrate i.e., $LiNO_3$ and KNO_3 [15], but weaker than the interactions observed in the uranyl or europium nitrate anions [14].

In the present study IRMPD spectra are recorded for $[M_2(NO_3)_5]^-$ clusters, where the cations are Mg^{2+}, Ca^{2+}, or Sr^{2+}. The larger group II nitrate clusters are investigated to gauge the effect of multiple metal centers on the position and degeneracy splitting of the antisymmetric nitrate stretch, and to compare the general values of ν_3 to those measured for the small, single cation species [17]. Exploration of cluster ions in the gas phase is an effective way to study the properties of nano-sized particles of matter, and in particular the transition from discrete atoms and molecules to bulk liquids and solids. The number of possible structures for a cluster ion increases rapidly with size and complexity. In the present case, the structures of the $[M_2(NO_3)_5]^-$ complexes are not known and isomers with multiple nitrate conformations are possible. Systematically altering the size of the metal cation offers the possibility of uncovering trends in nitrate binding, and by studying a mixed metal complex it may be possible to observe differences in metal-nitrate binding in the same spectrum.

Experimental

ESI FT-ICR Mass Spectrometry

Previously established methods are used for generation of ions and the subsequent collection of IRMPD spectra [14, 17]. Briefly, group II metal nitrate solutions are generated by dissolving the appropriate salt in water to produce primary standards each having a concentration of 10 mM, which are then further diluted with methanol in a 1:5 ratio. For the MgCa cluster, aliquots of the nitrate primary standards are mixed in a 1:1 ratio, and this solution is then diluted 1:5 with methanol. Ions of the formula $[M_2(NO_3)_5]^-$ (M_2 = Mg_2, MgCa, Ca_2, or Sr_2) are generated using ESI in a Micromass Z-Spray source. Ions are injected into a home-built Fourier transform ion cyclotron resonance (FT-ICR) mass spectrometer described in detail elsewhere [18].

Instrument operating parameters, such as desolvation temperature, cone voltage, and ion accumulation and transfer optics voltages, are optimized to maximize formation of $[M_2(NO_3)_5]^-$ and transfer of the species to the ICR cell. Dry nitrogen at a temperature of ~32 °C is used to assist in the desolvation process. Ions are accumulated for the duration of the previous FT-ICR cycle (~3 s) in an external hexapole and injected into the ICR cell via a quadrupole deflector and an octapole rf ion guide. Complexes of interest are isolated using a stored waveform inverse Fourier transform (SWIFT) pulse [19].

Infrared Multiple Photon Dissociation (IRMPD)

Infrared spectra are recorded by measuring the photodissociation yield as a function of photon wavelength. Precursor $[M_2(NO_3)_5]^-$ ions are irradiated using two FELIX macropulses (35 mJ per macropulse, 5 μs pulse duration, FWHM bandwidth ~0.5% of central λ). In the IRMPD process, a photon is absorbed when the laser frequency matches a vibrational mode of the gas-phase ion and its energy is subsequently distributed over all vibrational modes by intramolecular vibrational redistribution (IVR). The IVR process allows the energy of each photon to be dissipated before the ion absorbs another, which leads to the promotion of ion internal energy toward the dissociation threshold via multiple photon absorption [20]. It is important to note that studies have shown that infrared spectra obtained using IRMPD are comparable to those collected using linear absorption techniques [4, 21]. For the current experiments, the free electron laser wavelength is tuned between 6 and 12.5 μm in 0.1 to 0.04 μm increments. The intensity of product and un-dissociated precursor ions is measured using the excite/detect sequence of the FT-ICR-MS after each IRMPD step [22]. The IRMPD yield is normalized to the total ion current, and linearly corrected for variations in laser power across the range scanned [4, 19, 20].

DFT Geometry and Frequency Calculations

All DFT calculations are performed using the Gaussian 03 program, employing an approach similar to the one used in our previous group II nitrate study [17, 23–29]. Full geometry optimizations for $[Mg_2(NO_3)_5]^-$, $[Ca_2(NO_3)_5]^-$, and $[MgCa(NO_3)_5]^-$ are started using the B3LYP functional [24, 25] and the 3-21g* basis set. Initial optimization of $[Sr_2(NO_3)_5]^-$ is carried out with the MWB28 Stuttgart-Dresden (SDD)-type pseudopotential [26–29] and associated basis on the cation. To avoid bias, initial geometry optimizations were begun with nitrate and metal ion separated and randomly oriented, and the respective species were allowed to approach and find equilibrium positions as a result of the optimization process. As discussed further below, two stable structures have been identified, regardless of the initial structure used at the beginning of the conformation search. The first one is a mono-bridging isomer, $[M_2(bNO_3)(tNO_3)_4]^-$ that contains a single bridging nitrate ligand, and four terminal nitrate ligands. The second isomer is a structure containing three bridging nitrates, and two terminal nitrates, that we refer to as a tri-bridging isomer, $[M_2(bNO_3)_3(NO_3)_2]^-$.

The initial structures for $[Mg_2(NO_3)_5]^-$, $[Ca_2(NO_3)_5]^-$, and $[MgCa(NO_3)_5]^-$ are then re-optimized and frequency calculations are performed using the 6-311+G(2d),

6-311+G(3d), 6-311+G(2df) and 6-311+G(3df) basis sets. Re-optimization of, and frequency calculations for, $[Sr_2(NO_3)_5]^-$ involve use of the SDD pseudopotential on Sr and 6-311+G(2d), 6-311+G(3d), 6-311+G(2df) or 6-311+G(3df) basis sets on N and O. For comparison to IRMPD spectra, data generated at the B3LYP/6-311+G(3df) or B3LYP/MWB28/6-311+G(3df) level of theory are presented. For comparison to IRMPD spectra, the calculated frequencies were scaled by a factor of 0.98, which is customary for scaling calculations of this type [30–33].

Minima located using the approach outlined above are re-optimized using the PBEPBE, MPWPW91, and SVWN functionals and the 6-311+G(3df) or MWB28/6-311+G(3df) basis sets. Regardless of which functional is used, the trends outlined below with respect to the relative energies of the predicted conformational isomers are maintained. The same is true when MP2 single-point calculations are used to determine the relative energies of the minima located using B3LYP/6-311+G(3df) or B3LYP/MWB28/6-311+G(3df).

Results and Discussion

Density Functional Theory Calculations of Isomeric Complexes

Minima identified for $[Mg_2(NO_3)_5]^-$ are shown in Figure 1 and for the corresponding calcium, strontium and magnesium-calcium complexes in Figures S1–S4, (which can be found in the electronic version of this article) respectively. The mono-bridging structure is shown in Figure 1a and b and consists of one bridging nitrate ligand joining the two cations, and two terminal nitrate ligands on each cation. Table 1 shows the metal–oxygen bond lengths. Two different nitrates can thus be distinguished, the first being a terminal nitrate (t-NO_3) bound in a bidentate fashion to only one of the metal atoms. Terminal nitrates on the other metal atom are bound in a similar fashion. While there are two different pairs of terminal nitrate ligands, the structural difference is small and the calculations predict their vibrations to be near-degenerate, except for the magnesium-calcium mixed complex. The bridging ligand (b-NO_3) has one oxygen atom that is bound to both metal atoms, with the other two oxygen atoms bound to one of the metal atoms; i.e., each metal occupies adjacent O-N-O clefts on the bridging nitrate, which is referred to here as a double bidentate (db) nitrate bridge. The bond lengths between the nitrate ligands and the metal increase as the size of the metal increases, which suggests that the interaction between the metal and nitrate is stronger for the smaller, more charge-dense metals.

Figure 1c and d show the tri-bridging isomer, for which bond lengths are given in Table 2. This isomer contains nitrate anions in three different binding geometries: a terminal, non-bridging nitrate, and two different types of bridging nitrates. For one of the bridging nitrates adjacent O atoms are bound to each of the metal ions, and hence this is designated a double-monodentate (dm) nitrate bridge. In the second type of bridging nitrate, one metal cation occupies an O-N-O cleft, while the second metal is bound to a single O atom that is actually shared between both metal cations. This nitrate

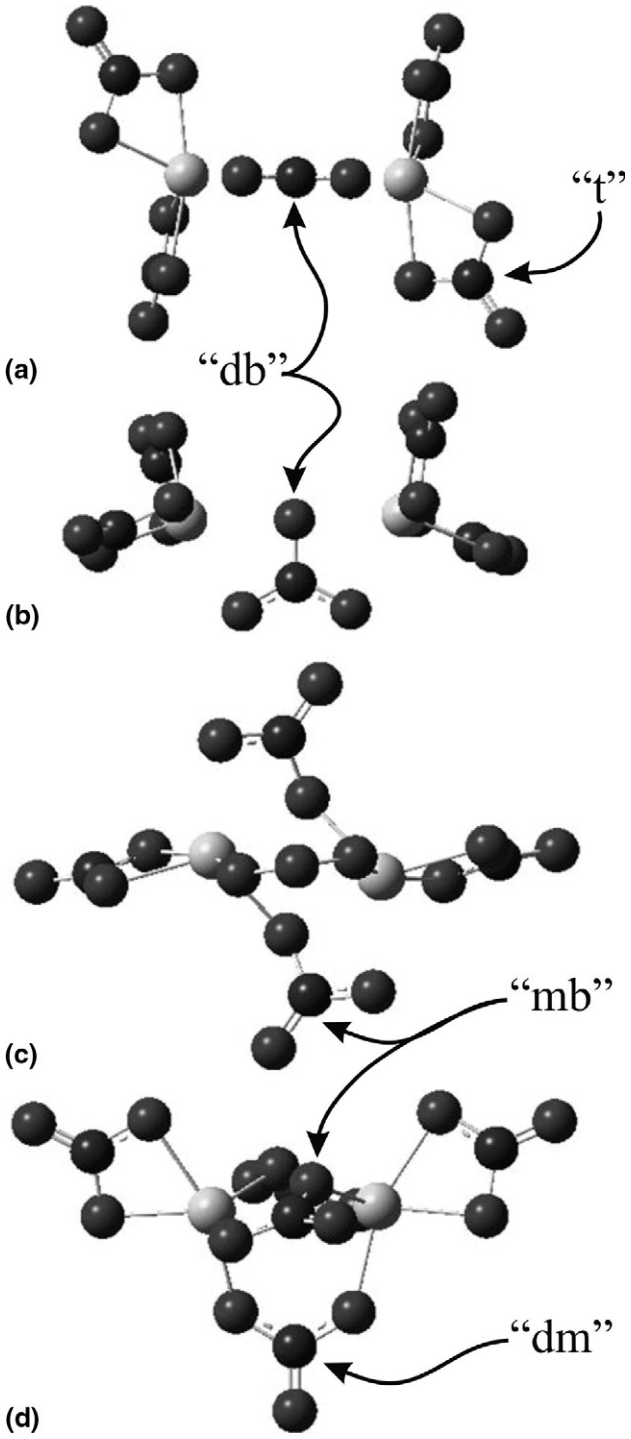

Figure 1. Optimized geometry of $[Mg_2(bNO_3)_1(tNO_3)_4]^-$ isomer (**a**) side view and (**b**) top view. Optimized geometry of $[Mg_2(bNO_3)_3(tNO_3)_2]^-$ isomer (**c**) side view and (**d**) top view. Structures were calculated with the B3LYP functional and the 6-311+G(3df) basis.

Table 1. Bond lengths for metal-oxygen bonds in mono-bridging $[M_2(bNO_3)(tNO_3)_4]^-$

Ion	M^1-O^8, M^2-O^{16}	M^1-O^{10}, M^2-O^{14}	M^1-O^{11}, M^2-O^{17}	M^1-O^{13}, M^2-O^{19}	M^1-O^{21}, M^2-O^{21}	M^1-O^{22}, M^2-O^{20}
$[Mg_2(NO_3)_5]^-$	2.069	2.072	2.078	2.072	2.208	2.208
$[Ca_2(NO_3)_5]^-$	2.348	2.361	2.351	2.361	2.513	2.490
$[Sr_2(NO_3)_5]^-$	2.510	2.519	2.512	2.519	2.693	2.650
$[Mg^1Ca^2(NO_3)_5]^-$	2.072, 2.346	2.074, 2.360	2.076, 2.351	2.075, 2.360	2.200, 2.515	2.194, 2.507

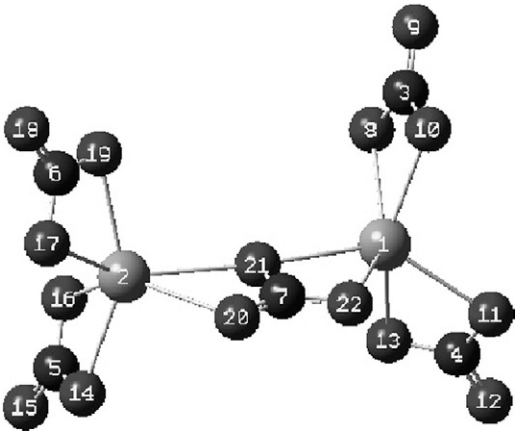

conformation is referred to as a monodentate-bidentate (mb) nitrate bridge.

The electronic energies and zero point corrections for both structures calculated at the B3LYP/6-311+G(3df) or B3LYP/MWB28/6-311+G(3df) level of theory are shown in Table 3. For each anionic cluster ion, the tri-bridging structure is lower in energy than the mono-bridging isomers, and the energy difference, ΔE, increases following the trend $[Mg_2(NO_3)_5]^- < [MgCa(NO_3)_5]^- < [Ca_2(NO_3)_5]^- < [Sr_2(NO_3)_5]^-$, with values ranging from 0.804 to 5.800 kcal/mol. We note that the same qualitative trend with respect to the relative energies of the respective isomers (mono-bridging versus tri-bridging) is observed regardless of the functional or basis set (6-311+G(2d), 6-311+G(3d), or 6-311+G(2df)) chosen, and when MP2 single point calculations are performed on the lowest energy structures predicted by DFT. Coupled cluster calculations [34–36] may provide a more accurate prediction of relative energies for these species.

IRMPD of $[M_2(NO_3)_5]^-$

The IRMPD spectra of $[Mg_2(NO_3)_5]^-$, $[Ca_2(NO_3)_5]^-$, and $[Sr_2(NO_3)_5]^-$ are shown in Figures 2, 3, and 4, respec-

Table 2. Bond lengths for metal-oxygen bonds in tri-bridging $[M_2(bNO_3)_3(tNO_3)_2]^-$

Ion	M^1-O^8, M^2-O^{13}	M^1-O^{10}, M^2-O^{11}	M^1-O^{16}, M^2-O^{19}	M^1-O^{17}, M^2-O^{14}	M^1-O^{19}, M^2-O^{16}	M^1-O^{20}, M^2-O^{22}
$[Mg_2(NO_3)_5]^-$	2.097	2.063	2.112	2.184	2.157	2.041
$[Ca_2(NO_3)_5]^-$	2.373	2.360	2.376	2.442	2.457	2.319
$[Sr_2(NO_3)_5]^-$	2.538	2.529	2.533	2.601	2.629	2.477
$[Mg^1Ca^2(NO_3)_5]^-$	2.109, 2.370	2.064, 2.361	2.097, 2.382	2.188, 2.440	2.165, 2.444	2.038, 2.318

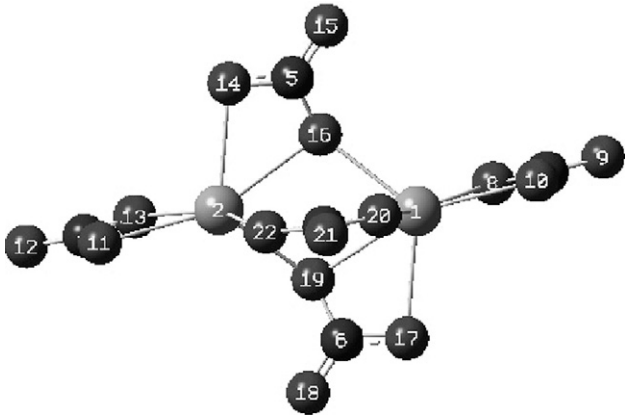

Table 3. Relative energies of $[M_2(NO_3)_5]^-$ conformational isomers

Structure	Electronic energy (hartrees)	Zero point correction (hartrees)	ZPE corrected energy (hartrees)	ΔE (kcal/mol)
$[Mg_2(bNO_3)_1(tNO_3)_4]^-$ mono-bridging	−1802.75646899	0.083139	−1802.673330	+0.804
$[Mg_2(bNO_3)_3(tNO_3)_2]^-$ tri-bridging	−1802.75803771	0.083426	−1802.674612	0
$[Ca_2(bNO_3)_1(tNO_3)_4]^-$ mono-bridging	−2757.83005434	0.079874	−2757.750181	+4.779
$[Ca_2(bNO_3)_3(tNO_3)_2]^-$ tri-bridging	−2757.83789177	0.080095	−2757.757797	0
$[Sr_2(bNO_3)_1(tNO_3)_4]^-$ mono-bridging	−1464.07150458	0.077997	−1463.993507	+5.800
$[Sr_2(bNO_3)_3(tNO_3)_2]^-$ tri-bridging	−1464.08082262	0.078073	−1464.002750	0
$[MgCa(bNO_3)_1(tNO_3)_4]^-$ mono-bridging	−2280.29375524	0.081521	−2280.212234	+2.374
$[MgCa(bNO_3)_3(tNO_3)_2]^-$ tri-bridging	−2280.29787779	0.081861	−2280.216017	0

tively, with the calculated spectra of the mono- and tri-bridging complexes in panels (b) and (c), and a weighted summation of both calculated spectra in panel (d). The IR spectrum of bare nitrate is known to feature a symmetric (ν_1) and an antisymmetric (ν_3) ONO stretch. Coordination to a metal ion causes the antisymmetric stretch mode to split into a low-frequency component due to the metal-bound O atoms and a high-frequency component due to the free O atoms [15, 16]. These modes are designated here as the bound and the free antisymmetric stretching modes, ν_{3b} and ν_{3f}, respectively. Moreover, because each complex contains five nitrate ligands, the observed features consist of a number of nearly degenerate bands, which are generally not resolved in the experiment. Table 4 shows the approximate values of the nitrate stretches in the IRMPD spectra for each of the complexes. The symmetric nitrate stretch is found between 1000 and 1060 cm^{-1} for each cluster anion: only a single vibration is observed in this region of the spectrum, except for the magnesium complex, for which two vibrations at 1007 and 1060 cm^{-1} are found. The values for ν_{3b}, ν_{3f}, and the magnitude of their splitting, $\Delta\nu_3$, are listed in Table 4. The largest splitting is observed for the magnesium complex and $\Delta\nu_3$ decreases as $[Mg_2(NO_3)_5]^- > [MgCa(NO_3)_5]^- > [Ca_2(NO_3)_5]^- > [Sr_2(NO_3)_5]^-$.

Table 5 shows the scaled frequencies (scaling factor of 0.98) for all of the degenerate ν_1, ν_{3b}, ν_{3f} absorption bands, and the $\Delta\nu_3$ calculated for the mono-bridging $[M_2(bNO_3)(tNO_3)_4]^-$ complexes at the B3LYP/6-311+G(3df) or B3LYP/MWB28/6-311+G(3df) level of theory. Calculated intensities are shown in bar format in Figures 2b–5b, and complete listings of all calculated frequencies and their intensities are provided in Tables S1–S4 in the Supplementary Information. Each of the three bands consists of a number of nearly, but not

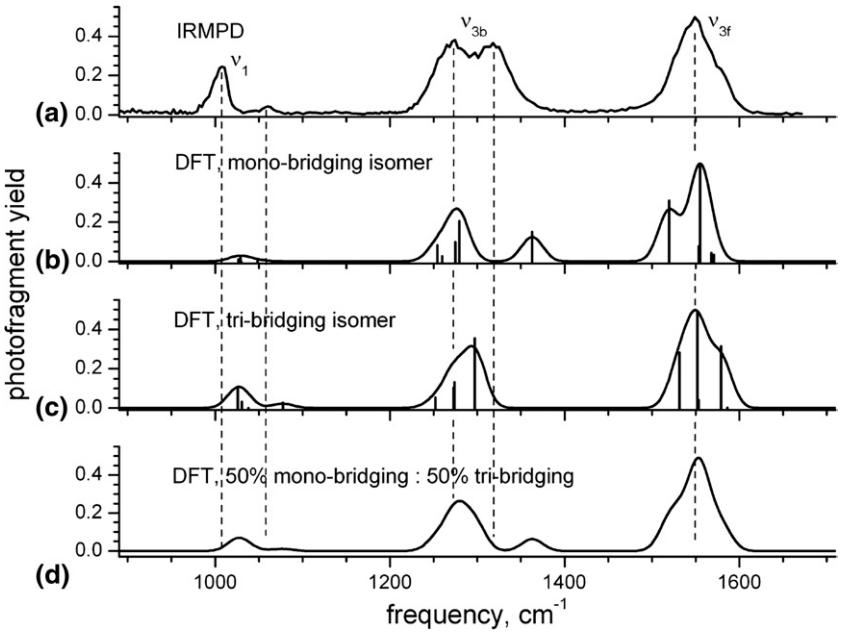

Figure 2. (**a**) IRMPD spectrum of $[Mg_2(NO_3)_5]^-$. (**b**) Calculated vibrational spectrum of the mono-bridging $[Mg_2(bNO_3)_1(tNO_3)_4]^-$ isomer. (**c**) Calculated vibrational spectrum of the tri-bridging $[Mg_2(bNO_3)_3(tNO_3)_2]^-$ isomer using the B3LYP functional and the 6-311+G(3df) basis. (**d**) A weighted summation of a 50:50 mixture of the spectra of the mono-bridging and tri-bridging isomers. In the calculated spectra (**b**) and (**c**), bars represent individual frequencies, while the smooth lines are Gaussian convolutions at the experimentally observed bandwidth.

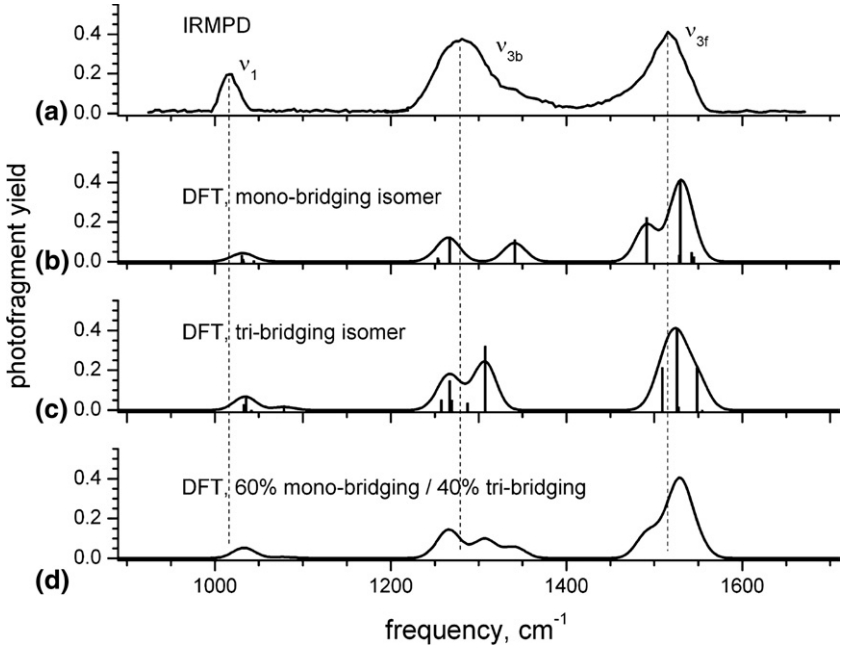

Figure 3. (**a**) IRMPD spectrum of $[Ca_2(NO_3)_5]^-$. (**b**) Calculated vibrational spectrum of the mono-bridging $[Ca_2(bNO_3)_1(tNO_3)_4]^-$ isomer. (**c**) Calculated vibrational spectrum of the tri-bridging $[Ca_2(bNO_3)_3(tNO_3)_2]^-$ isomer using the B3LYP functional and the 6-311+G(3df) basis. (**d**) A weighted summation of a 60:40 mixture of the spectra of the mono-bridging and tri-bridging isomers. In the calculated spectra (**b**) and (**c**), bars represent individual frequencies, while the smooth lines are Gaussian convolutions at the experimentally observed bandwidth.

exactly degenerate vibrations, because the structures of the five ligands in the complex are not identical, and so their vibrations are slightly different. For the mono-bridging conformation, the ν_1 symmetric nitrate stretch is predicted to appear as a single absorption, regardless of the complex. The ν_{3b} vibrations are observed at ca. 1280–1300 cm^{-1}, which correspond to the terminal nitrate ligands, and also at 1340–1360 cm^{-1}, which correspond to the bridging nitrate ligand. The major ν_{3f} bands occur between 1470 and 1560 cm^{-1}, depending on the chemical environment.

Table 6 shows the scaled frequencies (factor 0.98) for all of the degenerate ν_1, ν_{3b}, ν_{3f} bands for the tri-bridging $[M_2(bNO_3)_3(tNO_3)_2]^-$ isomer. Calculated intensities are shown in bar format in Figures 2c–5c, and complete listings of all calculated frequencies and their intensities are provided in Tables S1–S4 in the Supplementary Information. The symmetric ν_1 bands are found between 1020 and 1070 cm^{-1} and now appear as two peaks, the more intense peak corresponding to the symmetric nitrate stretch of the terminal and monodentate-bidentate bridging nitrate ligands, t-NO_3 and mb-NO_3, respectively. The double-monodentate nitrate bridge, dm-NO_3, produces a less intense peak shifted to higher frequency by ~50 cm^{-1}. The antisymmetric ν_{3b} stretching vibrations are calculated between 1250 and 1320 cm^{-1}. Near degeneracy of the modes on the various nitrate ligands causes a splitting into multiple closely spaced peaks, indicating similarity between the chemical environments and consequent structures of the nitrate ligands. The antisymmetric ν_{3f} is found between 1490 and 1580 cm^{-1} and is also split into multiple near degenerate bands.

The IRMPD spectrum of $[Mg_2(NO_3)_5]^-$ (Figure 2a) is compared with the spectra calculated for the two isomers to gain insight into possible structures of the complex. The peaks at ca. 1007 and 1060 cm^{-1} are attributed to the ν_1 stretch. The predicted spectrum for the tri-bridging isomer (Figure 2c) contains both peaks although at frequencies ~20 cm^{-1} higher than the measurement. The spectrum calculated for the mono-bridging complex (Figure 2b) contains only a single peak in this region of the spectrum. Agreement between the experimental and calculated frequencies for the ν_{3b} stretch is not as good: the IRMPD ν_{3b} region contains two modestly-resolved peaks at ca. 1270 and 1320 cm^{-1}. The broadened profiles of these peaks suggest contributions from multiple, unresolved components. The predicted spectrum for the tri-bridging complex has four bands ranging from 1252 to 1297 cm^{-1} in this region. Gaussian convolution of these frequencies using bandwidths similar to those seen in the IRMPD spectrum shows that these peaks are likely not resolved in the experiment. Turning to the mono-bridging complex, five different ν_{3b} bands are calculated, with the most intense at 1280 cm^{-1}. This peak is in good agreement with one of the experimental bands, but the calculated band at 1363 cm^{-1} is not observed in the experimental spectrum. The antisymmetric ν_{3f} band is a fairly broad resonance centered at 1549 cm^{-1}, and calculated spectra

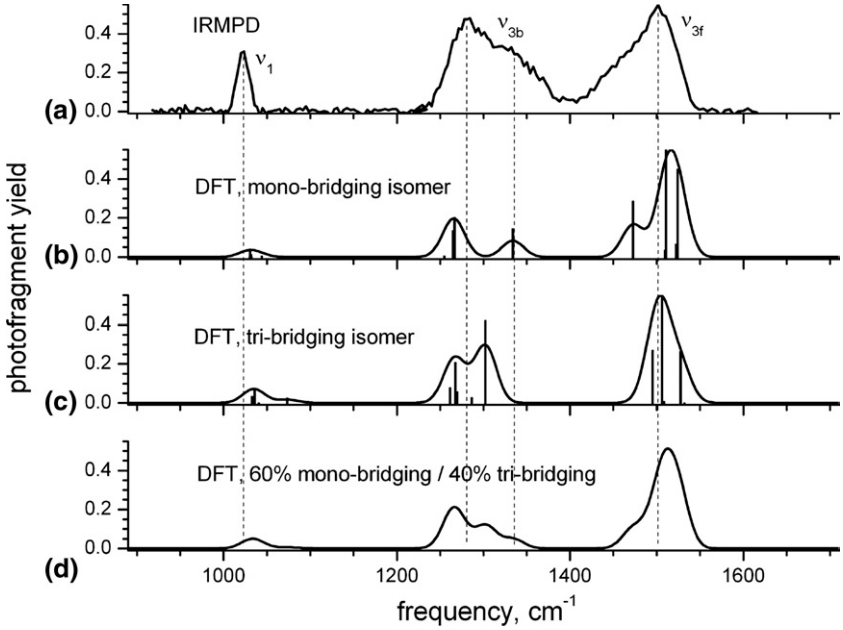

Figure 4. (**a**) IRMPD spectrum of $[Sr_2(NO_3)_5]^-$. (**b**) Calculated vibrational spectrum of the mono-bridging $[Sr_2(bNO_3)_1(tNO_3)_4]^-$ isomer. (**c**) Calculated vibrational spectrum of the tri-bridging $[Sr_2(bNO_3)_3(tNO_3)_2]^-$ isomer using B3LYP functional and the MWB28/6-311+G(3df) basis for Sr/N,O. (**d**) A weighted summation of a 60:40 mixture of the spectra of the mono-bridging and tri-bridging isomers. In the calculated spectra (**b**) and (**c**), bars represent individual frequencies, while the smooth lines are Gaussian convolutions at the experimentally observed bandwidth.

for both structures provide reasonable agreement in this region. The tri-bridging isomer is calculated to have three absorptions that would not be resolved in the experiment, but would have a high-frequency shoulder at about 1580 cm^{-1}, which is in good qualitative agreement with the profile of the IRMPD spectrum. Conversely, the spectrum calculated for the mono-bridging structure has a second absorption at 1520 cm^{-1}, that should be resolved from the major component at 1554 cm^{-1}, but this is not seen. An alternative method for comparing structures is to compare experimental and calculated $\Delta\nu_3$ values, measured as 254 cm^{-1}. The difference of the un-weighted averages calculated for the ν_{3b} and ν_{3f} frequencies gives values that are about 20 cm^{-1} higher for both the tri-bridging and mono-bridging structures, and so in this case, consideration of $\Delta\nu_3$ does not provide additional insight.

The overall spectral profile is in better agreement with that of the tri-bridging isomer in accord with the lower energy of this structure. However, the calculated spectrum is not in perfect agreement, particularly with the ν_{3b} modes. Possibly, both tri- and mono-bridging isomers are present, which is reasonable given the small energy difference between the isomers. A synthesized spectrum for a 50:50 mixture of the two isomers (Figure 2d) provides good agreement for the ν_{3f} and ν_1 modes, but contains an unobserved band at ~1360 cm^{-1}. Thus,

Table 4. Centroids for peaks in IRMPD spectra of $[M_2(NO_3)_5]^-$

Ion	N=O (ν_3)	O-N-O (ν_3)	$\Delta\nu_3$	Sym. NO_3 (ν_1)
$[Mg_2(NO_3)_5]^-$	1549	1272, 1318	254	1007, 1060
$[Ca_2(NO_3)_5]^-$	1516	1282	234	1016
$[Sr_2(NO_3)_5]^-$	1500	1280	220	1023
$[MgCa(NO_3)_5]^-$	1524, 1549	1266, 1295	243	1009

Table 5. Scaled vibrational frequencies for $[M_2(bNO_3)(tNO_3)_4]^-$ using DFT

Ion	High frequency ν_3	Low frequency ν_3	$\Delta\nu_3$	Sym. NO_3 (ν_1)
$[Mg_2(NO_3)_5]^-$	1519.45[b]	1254.35	272.50	1026.65
	1553.60	1259.76		1026.74
	1555.01	1274.91		1028.87
	1567.99	1279.78		1029.73
	1570.86	1362.84[b]		1048.53[b]
$[Ca_2(NO_3)_5]^-$	1491.28[b]	1253.67	255.56	1030.38
	1528.31	1254.73		1030.52
	1529.51	1267.21		1031.79
	1542.25	1267.24		1032.46
	1544.921	1341.18[b]		1044.51[b]
$[Sr_2(NO_3)_5]^-$	1472.57[b]	1254.66	237.81	1030.51
	1509.55	1254.77		1030.63
	1510.65	1264.88		1031.83
	1522.35	1266.48		1032.41
	1524.84	1333.91[b]		1044.34[b]
$[MgCa(NO_3)_5]^-$	1507.36[b]	1254.09	264.50	1026.64[Mg]
	1528.61[Ca]	1257.35		1029.13[Mg]
	1543.92[Ca]	1268.32[Ca]		1030.83[Ca]
	1554.57[Mg]	1276.65[Mg]		1032.53[Ca]
	1569.32[Mg]	1351.36[b]		1045.92[b]

[b] = vibration of a bridging nitrate ligand.
[Mg] = vibration of nitrate ligands bonded to magnesium.
[Ca] = vibration of nitrate ligand bonded to calcium.

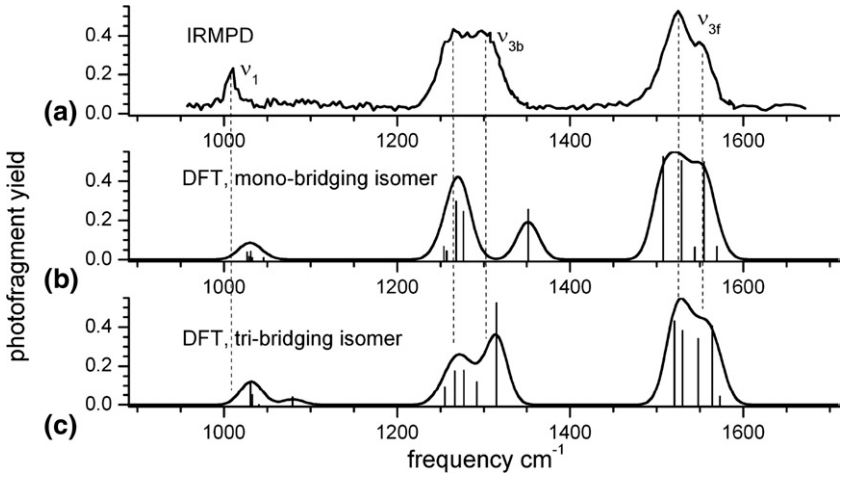

Figure 5. (**a**) IRMPD spectrum of $[MgCa(NO_3)_5]^-$. (**b**) Calculated vibrational spectrum of the mono-bridging $[MgCa(bNO_3)_1(tNO_3)_4]^-$ isomer. (**c**) Calculated vibrational spectrum of the tri-bridging $[MgCa(bNO_3)_3(tNO_3)_2]^-$ isomer using the B3LYP functional and the 6-311+G(3df) basis. In the calculated spectra (**b**) and (**c**), bars represent individual frequencies, while the smooth lines are Gaussian convolutions at the experimentally observed bandwidth.

the observed ν_{3b} band at ~1320 cm^{-1} is not well reproduced by either of the models: this peak suggests the presence of a nitrate that is less symmetric than the db-nitrate responsible for the ν_{3b} peak calculated at 1360 cm^{-1}, but is more symmetric than the mb-nitrate which produces ν_{3b} frequencies in the 1280–1300 cm^{-1} range. Inclusion of a nitrate moiety having intermediate symmetry would represent a significant geometry alteration compared with either the mono-bridging or tri-bridging structures, and we were unable to computationally identify such minima.

The IRMPD spectrum of $[Ca_2(NO_3)_5]^-$ (Figure 3) shows only a single ν_1 peak at 1016 cm^{-1}. The calculated spectrum for the mono-bridging structure produces a peak at 1030 cm^{-1}, while two peaks were calculated (1035 and 1079 cm^{-1}) for the tri-bridging structure. As in the case of the Mg_2 cluster, agreement in the ν_{3b} region is relatively poor for either structure. The experimental spectrum contains a noticeably broadened ν_{3b} band centered at ~1282 cm^{-1} with a high-frequency shoulder. The calculated spectrum for the tri-bridging structure (Figure 3c) shows two closely spaced peaks at 1267 and 1308 cm^{-1} that are modestly resolved when convoluted with band profiles similar to those found in the experimental spectrum, and further broadening of this model would give a reasonable match to the main band

Table 6. Scaled vibrational frequencies for $[M_2(bNO_3)_3(tNO_3)_2]^-$ using DFT

Ion	High frequency ν_3	Low frequency ν_3	$\Delta\nu_3$	Sym. NO_3 (ν_1)
$[Mg_2(NO_3)_5]^-$	1531.51^{dm}	$1252.06^{t,mb,dm}$	267.13	1025.74^{mb}
	1522.42^{t}	$1273.07^{t,mb}$		1030.60^{t}
	$1553.14^{t,mb}$	$1297.14^{t,mb}$		1077.43^{dm}
	1579.14^{mb}	$1316.83^{t,mb,dm}$		
$[Ca_2(NO_3)_5]^-$	1509.10^{dm}	$1257.80^{t,mb,dm}$	254.91	1032.58^{t}
	1525.83^{t}	1267.35^{t}		1032.90^{t}
	$1527.64^{t,mb}$	$1269.62^{t,mb,dm}$		1035.31^{mb}
	1548.59^{mb}	1287.52^{mb}		1078.69^{dm}
		$1307.58^{mb,dm}$		
$[Sr_2(NO_3)_5]^-$	1495.24^{dm}	$1261.50^{t,mb,dm}$	236.54	1033.11^{t}
	1506.06^{t}	1267.43^{t}		1033.32^{t}
	$1508.27^{t,mb}$	$1269.47^{t,mb,dm}$		1035.87^{mb}
	1527.47^{mb}	1286.43^{mb}		1073.61^{dm}
		$1302.42^{mb,dm}$		
$[MgCa(NO_3)_5]^-$	1520.43^{dm}	$1255.30^{t,mb,dm}$	264.68	$1030.66^{t,mb}$
	$1529.71^{t(Ca)}$	$1266.44^{t(Ca),mb(Ca)}$		$1032.78^{t,mb}$
	$1547.89^{t(Mg)}$	$1276.97^{t(Mg),mb(Mg)}$		1079.42^{dm}
	1564.11^{mb}	$1292.13^{t,mb,dm}$		
		$1314.88^{t,mb,dm}$		

^{t} = vibration of terminal nitrate ligands.
^{mb} = vibration of monodentate-bidentate bridging nitrate ligands.
^{dm} = vibration of double monodentate binding bridging nitrate ligand.

observed. As in the spectrum calculated for the Mg_2 mono-bridging isomer, the Ca_2 mono-bridging isomer displays two well-resolved ν_{3b} peaks at 1267 cm^{-1} and 1341 cm^{-1}. Considering ν_{3f}, we see another broadened peak centered at about 1516 cm^{-1}, with a prominent shoulder on the low-frequency side. The two ν_{3f} bands calculated for the mono-bridging isomer would produce such a shoulder, although somewhat better resolution would be expected given the experimental peak widths, and this is not observed. Three significant ν_{3f} components are calculated for the tri-bridging isomer, which when convoluted show a ν_{3f} profile with a high-frequency shoulder, not in accord with the IRMPD spectrum. In this instance a spectrum synthesized from a 60:40 weighted summation of the mono-bridging and tri-bridging isomers provides better qualitative agreement with the experimental spectrum. Correctly oriented shoulders are generated on both the ν_{3b} and ν_{3f} bands. Thus, for $[Ca_2(NO_3)_5]^-$ the correlation between the experimental IR spectrum and the theoretical spectrum generated by weighted summation strongly suggests that a mixture of isomers is present.

The IRMPD spectrum of $[Sr_2(NO_3)_5]^-$ (Figure 4a) again shows three prominent peaks due to the symmetric ν_1 and antisymmetric ν_{3b} and ν_{3f} nitrate stretching modes. The ν_1 mode measured at ~1020 cm^{-1} is reasonably reproduced in the spectra calculated for both the mono-bridging and tri-bridging structures, however, the latter also is predicted to possess a lower intensity ν_1 peak about 40 cm^{-1} higher that is not seen experimentally. The ν_{3b} region of the IRMPD consists of a broadened profile, indicative of multiple unresolved components, centered at ~1280 cm^{-1}, with a second maximum at ~1335 cm^{-1}. The calculated spectrum for the mono-bridging isomer has two peaks in the ν_{3b} region that provide a qualitative fit, although better resolution might have been expected. The calculated spectrum for the tri-bridging structure also shows two (nearly) resolved ν_{3b} peaks, but their relative intensities are counter to those observed experimentally. Considering the ν_{3f} region, agreement between experiment and calculated spectra appears better for the mono-bridging isomer: the three ν_{3f} components calculated produce a profile with a shoulder to lower frequencies in accord with the IRMPD spectrum, although again somewhat better resolution might have been expected. The tri-bridging isomer has three unresolved bands matching with the main band observed, but the shoulder to lower frequencies is not reproduced. A weighted 60:40 summation of the spectra of the mono-bridging and tri-bridging structures provides better qualitative agreement with the IRMPD profiles measured for both the ν_{3b} and ν_{3f} regions (Figure 4d) and provides a reasonable explanation for the broadened profiles. The mono-bridging structure is calculated to be <6 kcal/mol higher than the tri-bridging structure, which again indicates potential inaccuracy of the energies for the species calculated by DFT, and the need for improvement in this area.

IRMPD of $[MgCa(NO_3)_5]^-$

Figure 5 shows the IRMPD spectrum of the mixed-metal $[MgCa(NO_3)_5]^-$ complex as well as calculated spectra for the mono- and tri-bridging isomers. IR induced dissociation of $[MgCa(NO_3)_5]^-$ leads to the formation of both $[Mg(NO_3)_3]^-$ and $[Ca(NO_3)_3]^-$, see Scheme **1**. The trinitrato-calcium anion is generated in a ~2:1 ratio to the trinitrato-magnesium anion. At first glance, this result appears counterintuitive, since the $\Delta\nu_3$ values indicate a stronger interaction between nitrate and magnesium than between nitrate and calcium. This supposition is supported by an analysis of the metal–oxygen bond lengths (Tables 1 and 2 for the mono-bridging and tri-bridging structures, respectively), which show that the Mg–O distances are shorter than the corresponding Ca–O distances. However, relative energies for the ionic and neutral products for each reaction shown in Scheme **1** were calculated at the B3LYP/6-311+G(3df) level of theory, and formation of the trinitrato-calcium anion was found to be favored by 1.124 kcal/mol. Previous work by our group indicates that the magnesium complex adopts a conformation in which the nitrate ligands are significantly tilted to alleviate the ligand-ligand repulsive interactions [17]. Thus, it is expected that minimizing the number of nitrate ligands on the Mg cation serves to minimize these repulsive forces, and hence the formation of the neutral $[Mg(NO_3)_2]$ and the anionic $[Ca(NO_3)_3]^-$ is favored.

The ν_1 band of $[MgCa(NO_3)_5]^-$ (Figure 5a) is centered at 1009 cm^{-1}, in reasonable agreement with values calculated for the tri-bridging and mono-bridging complexes. The tri-bridging complex is predicted to have an additional ν_1 stretch at about 1080 cm^{-1} that was not observed experimentally. However, the lower signal to noise ratio for the mixed-metal complex may have prevented observation of this second, relatively weak absorption. The ν_{3b} region of the IRMPD spectrum is a broadened, flat-topped peak that can be considered to be derived from closely-spaced, unresolved peaks centered between ~1265 and ~1300 cm^{-1}. The calculated spectrum for the tri-bridging isomer clearly mimics this band shape better than that for the mono-bridging one. The mono-bridging isomer has three salient frequency components, two of which are calculated within the range defined by the IRMPD ν_{3b} profile, but one at ~1350 cm^{-1}, which is not observed experimentally. Agreement between experiment and theory for the ν_{3f} region, where a broadened peak centered at ~1524

$$[MgCa(NO_3)_5]^- \rightarrow [Mg(NO_3)_3]^- + [Ca(NO_3)_2]^0$$
$$[MgCa(NO_3)_5]^- \rightarrow [Ca(NO_3)_3]^- + [Mg(NO_3)_2]^0$$

Scheme 1. Dissociation pathway of mixed magnesium/calcium nitrate cluster anion.

cm^{-1} with a second maximum at about 1549 cm^{-1} is observed, is also better for the tri-bridging isomer than for the mono-bridging version. The experimental $\Delta\nu_3$ value is about 243 cm^{-1}, smaller than the value for the magnesium dimer but larger than that for the calcium dimer.

Conclusions

Group II nitrate clusters of the formula $[M_2(NO_3)_5]^-$ (M = Mg_2, MgCa, Ca_2, or Sr_2) were studied using IRMPD spectroscopy by measuring the yield of $[M(NO_3)_3]^-$ as a function of wavelength. The IRMPD spectra of all four complexes display prominent absorption bands corresponding to ν_1 and split ν_3 vibrations, the latter being designated as lower frequency ν_{3b} (representing the antisymmetric stretch of the O-N-O moiety bound to the metal) and the higher frequency ν_{3f} (representing the antisymmetric stretch of the non-metal bonding, or free nitrosyl moiety). The magnitude of the splitting, $\Delta\nu_3$, indicates that the strength of the interaction between the metal and ligand decreases according to $[Mg_2(NO_3)_5]^- > [MgCa(NO_3)_5]^- > [Ca_2(NO_3)_5]^- > [Sr_2(NO_3)_5]^-$. The band frequencies vary depending on the metal, indicating that values reflect changes in structure or strength of binding.

DFT calculations were performed to elucidate structural implications, and two stable structures were calculated for all four complexes: a mono-bridging structure in which the two metals are bound by a single nitrate, with four non-bridging (or terminal nitrates), and a tri-bridging structure, in which the two metals are bound by three nitrates, with two non-bridging nitrate ligands.

In the case of the Mg_2 and MgCa clusters, the spectral profiles calculated for the tri-bridging and mono-bridging structures are in poor agreement with the experimental IRMPD spectrum. The creation of a weighted summation of the two structures provides some evidence for existence of a mixture of species, and of an alternative nitrate ligand that is more symmetrical than the terminal nitrates, but not as symmetrical as the db-nitrate modeled in the mono-bridging structure. We have however not been able to locate stable structures of this sort on the potential energy surface.

The IRMPD spectra of the Ca_2 and Sr_2 complexes are in good agreement with spectra synthesized from a 60:40 weighted summation of spectra calculated for the mono-bridging and tri-bridging structures, respectively. The summed spectra reproduce frequency and qualitative profiles of all three spectroscopic features. This suggests that the ion population of these complexes consists of a mixture of at least two structures, which may also explain the more broadened, unresolved appearance of the IRMPD spectra. The MgCa complex clearly favors a tri-bridging structure over a mono-bridging one, in agreement with the calculated energetics.

The relative energies of the isomers indicate that a mixture of structures is a reasonable possibility. The DFT calculations indicate that the tri-bridging structures are lower in energy than the mono-bridging structures, but never by more than 5.8 kcal/mol. The energy difference between the two structures increases as $[Mg_2(NO_3)_5]^- < [MgCa(NO_3)_5]^- < [Ca_2(NO_3)_5]^- < [Sr_2(NO_3)_5]^-$. In the Ca_2 and Sr_2 complexes, the summed DFT spectra suggest that the higher energy mono-bridging complex may be more abundant than the tri-bridging complex.

Acknowledgments

Work by CML, RPD, and MVS is supported in part by a grant from the U.S. National Science Foundation (NSF grant CAREER-0239800) and the Fairmount College of Liberal Arts and Sciences of Wichita State University. Density functional theory calculations were performed at Wichita State University using resources of the High-Performance Computing Center (HIPECC), a facility supported by the NSF under grants EIA-0216178 and EPS-0236913 and matching support from the State of Kansas and HIPECC. Work by GSG (under the INL LDRD Program) and the use of the INL High-Performance Computing Cluster, are supported by the U.S. Department of Energy, Idaho National Laboratory, DOE Idaho Operations Office contract DE AC07 05ID14517. JO and JS are supported by the Nederlandse Organisatie voor Wetenschappelijk Onderzoek (NWO). Construction and shipping of the FT-ICR-MS instrument was made possible through funding from the National High Field FT-ICR Facility (grant CHE-9909502) at the National High Magnetic Field Laboratory, Tallahassee, FL. The authors gratefully acknowledge the excellent support by Dr. B. Redlich and others of the FELIX staff is.

Appendix A. Supplementary Material

Supplementary material associated with this article may be found in the online version at doi:10.1016/j.jasms.2008.12.023.

References

1. Oomens, J.; Sartakov, B. G.; Meijer, G.; von Helden, G. Gas-Phase Infrared Multiple Photon Dissociation Spectroscopy of Mass-selected Molecular Ions. *Int. J. Mass Spectrom.* **2006,** *254,* 1–19.
2. Moore, D. T.; Oomens J.; Eyler, J. R.; Meijer, G.; von Helden, G.; Ridge, D. P. Gas-Phase IR Spectroscopy of Anionic Iron Carbonyl Clusters. *J. Am. Chem. Soc.* **2004,** *126,* 14726–14727.
3. Oomens, J.; Moore, D. T.; von Helden, G.; Meijer, G.; Dunbar, R. C. The Site of Cr^+ Attachment to Gas-Phase Aniline from Infrared Spectroscopy. *J. Am. Chem. Soc.* **2004,** *126,* 724–725.
4. Moore, D. T.; Oomens, J.; Eyler, J. R.; von Helden, G.; Meijer, G.; Dunbar, R. C. Infrared Spectroscopy of Gas-Phase Cr^+ Coordination Complexes: Determination of Binding Sites and Electronic States. *J. Am. Chem. Soc.* **2005,** *127,* 7243–7254.
5. Fielicke, A.; von Helden, G.; Meijer, G.; Pedersen, D. B.; Simard, B.; Rayner, D. M. Size and Charge Effects on the Binding of CO to Small Isolated Rhodium Clusters. *J. Phys. Chem. B* **2004,** *108,* 14591–14598.
6. Reinhard, B. M.; Lagutschenkov, A.; Lemaire, J.; Maitre, P.; Boissel, P.; Neidner-Schatteburg, G. Reductive Nitrile Coupling in Niobium-Acetonitrile Complexes Probed by Free Electron Laser IR Multiphoton Dissociation Spectroscopy. *J. Phys. Chem. A* **2004,** *108,* 3350–3355.
7. Jaeger, T. D.; van Heijnsbergen, D.; Klippenstein, S. J.; von Helden, G.; Meijer, G.; Duncan, M. A. Vibrational Spectroscopy and Density Functional Theory of Transition-Metal Ion-Benzene and Dibenzene Complexes in the Gas Phase. *J. Am. Chem. Soc.* **2004,** *126,* 10981–10991.
8. van Heijnsbergen, D.; von Helden, G.; Meijer, G.; Maitre, P.; Duncan, M. A. Infrared Spectra of Gas-Phase V^+-(Benzene) and V^+-$(Benzene)_2$ Complexes. *J. Am. Chem. Soc.* **2002,** *124,* 1562–1563.
9. Polfer, N. C.; Oomens, J.; Dunbar, R. C. IRMPD. Spectroscopy of Metal-Ion/Tryptophan Complexes. *Phys. Chem-Chem. Phys.* **2006,** *8,* 2744–2751.

10. Groenewold, G. S.; Gianotto, A. K.; Cossel, K. C.; Van Stipdonk, M. J.; Moore, D. T.; Polfer, N.; Oomens, J.; de Jong, W. A.; Visscher, L. Vibrational Spectroscopy of Mass-Selected $[UO_2(ligand)_n]^{2+}$ Complexes in the Gas Phase: Comparison with Theory. *J. Am. Chem. Soc.* **2006,** *128,* 4802–4813.
11. Duncan, M. A. Spectroscopy of Metal Ion Complexes: Gas-Phase Models for Solvation. *Ann. Rev. Phys. Chem.* **1997,** *48,* 69–93.
12. Duncan, M. A. Infrared Spectroscopy to Probe Structure and Dynamics in Metal Ion-Molecule Complexes. *Int. Rev. Phys. Chem.* **2003,** *22,* 407–435.
13. Lemaire, J.; Boissel, M.; Heninger, M.; Mauclaire, G.; Bellec, G.; Mestdagh, H.; Simon, A.; Le Caer, S.; Ortega, J. M.; Glotin F.; Maitre, P. Gas Phase Infrared Spectroscopy of Selectively Prepared Ions. *Phys. Rev. Lett.* **2002,** *89,* 273002/1–273002/4.
14. Groenewold, G. S.; Oomens, J.; de Jong, W. A.; Gresham, G. L.; McIlwain, M. E.; Van Stipdonk, M. J. Vibrational Spectroscopy of Anionic Nitrate Complexes of UO_2^{2+} and Eu^{3+} Isolated in the Gas Phase. *Phys. Chem., Chem. Phys.* **2008,** *10,* 1192–1202.
15. Smith, D.; James, D. W.; Devlin, J. P. Vibrational Spectra of Molecular Metal Nitrate Monomers and Dimers. *J. Chem. Phys.* **1971,** *54,* 4437–4442.
16. Ritzhaupt, G.; Devlin, J. P. Ionic Versus Molecular Nature of Monomeric Ammonium and Hydronium Nitrate. Infrared Spectra of Hydronium Nitrate ($H_3O + NO_3^-$) and Ammonium Nitrate ($NH_4 + NO_3^-$) Solvated in Argon Matrices. *J. Phys. Chem.* **1977,** *81,* 521–525.
17. Oomens, J.; Myers, L.; Dain, R.; Leavitt, C.; Pham, V.; Gresham, G.; Groenewold, G.; Van Stipdonk, M. Infrared Multiple-Photon Photodissociation of Gas-Phase Group II Metal-Nitrate Anions. *Int. J. Mass Spectrom.* **2008,** *273,* 24–30.
18. Valle, J. J.; Eyler, J. R.; Oomens, J.; Moore, D. T.; van der Meer, A. F. G.; von Helden, G.; Meijer, G.; Hendrickson, C. L.; Marshall, A. G.; Blakney, G. T. Free Electron Laser-Fourier Transform Ion Cyclotron Resonance Mass Spectrometry Facility for Obtaining Infrared Multiphoton Dissociation Spectra of Gaseous Ions. *Rev. Sci. Instrum.* **2005,** *76,* 023103/1–023103/7.
19. Marshall, A. G.; Wang, T. C. L.; Ricca, T. L. Tailored Excitation for Fourier Transform Ion Cyclotron Mass Spectrometry. *J. Am. Chem. Soc.* **1985,** *107,* 7893–7987.
20. Bagratashvili, V. N.; Letokov, V. S.; Makarov, A. A.; Ryabov, E. A. Multiple Photon Infrared Laser Photophysics and Photochemistry; Harwood: Chur, Switzerland, 1985.
21. Oomens, J.; Tielens, A G. G. M.; Sartakov, B. G.; von Helden, G.; Meijer, G. Laboratory Infrared Spectroscopy of Cationic Polycyclic Aromatic Hydrocarbon Molecules. *Astrophys. J.* **2003,** *591,* 968–985.
22. Marshall, A. G.; Hendrickson, C. L.; Jackson, G. S. Fourier Transform Ion Cyclotron Resonance Mass Spectrometry: A Primer. *Mass Spectrom. Rev.* **1998,** *17,* 1–35.
23. Frisch, M. J.; Trucks, G. W.; Schlegel, H. B.; Scuseria, G. E.; Robb, M. A.; Cheeseman, J. R.; Montgomery, J. A. Jr.; Vreven, T.; Kudin, K. N.; Burant, J. C.; Millam, J. M.; Iyengar, S. S.; Tomasi, J.; Barone, V.; Mennucci, B.; Cossi, M.; Scalmani, G.; Rega, N.; Petersson, G. A.; Nakatsuji, H.; Hada, M.; Ehara, M.; Toyota, K.; Fukuda, R.; Hasegawa, J.; Ishida, M.; Nakajima, T.; Honda, Y.; Kitao, O.; Nakai, H.; Klene, M.; Li, X.; Knox, J. E.; Hratchian, H. P.; Cross, J. B.; Bakken, V.; Adamo, C.; Jaramillo, J.; Gomperts, R.; Stratmann, R. E.; Yazyev, O.; Austin, A. J.; Cammi, R.; Pomelli, C.; Ochterski, J. W.; Y. Ayala, P.; Morokuma, K.; Voth, G. A.; Salvador, P.; Dannenberg, J. J.; Zakrzewski, V. G.; Dapprich, S.; Daniels, A. D.; Strain, M. C.; Farkas, O.; Malick, D. K.; Rabuck, A. D.; Raghavachari, K.; Foresman, J. B.; Ortiz, J. V.; Cui, Q.; Baboul, A. G.; Clifford, S.; Cioslowski, J.; Stefanov, B. B.; Liu, G.; Liashenko, A.; Piskorz, P.; Komaromi, I.; Martin, R. L.; Fox, D. J.; Keith, T.; Al-Laham, M. A.; Peng, C. Y.; Nanayakkara, A.; Challacombe, M.; Gill, P. M. W.; Johnson, B.; Chen, W.; Wong, M. W.; Gonzalez, C.; Pople, J. A. *Gaussian 03* Revision D.01; Gaussian, Inc.: Wallingford CT, 2004.
24. Lee, C.; Yang, W.; Parr, R. G. Development of the Colle-Salvetti Correlation-Energy Formula into a Functional of the Electron Density. *Phys. Rev. B* **1988,** *37,* 785–789.
25. Becke, A. D. Density-Functional Thermochemistry. III. The Role of Exact Exchange. *J. Chem. Phys.* **1993,** *98,* 5648–5652.
26. Bergner, A.; Dolg, M.; Kuchle, W.; Stoll, H.; Preuss, H. Ab Initio Energy-Adjusted Pseudopotentials for Elements of Groups 13–17. *Mol. Phys.* **1993,** *80,* 1431–1441.
27. Dolg, M.; Stoll, H.; Preuss, H.; Pitzer, R. M. Relativistic and Correlation Effects for Element 105 (Hahnium, Ha): A Comparative Study of M and MO (M = Nb, Ta, Ha) Using Energy-Adjusted Ab Initio Pseudopotentials. *J. Phys. Chem.* **1993,** *97,* 5852–5859.
28. Kuchle, W.; Dolg, M.; Stoll, H.; Preuss, H. Ab Initio Pseudopotentials for Mercury through Radon. I. Parameter Sets and Atomic Calculations. *Mol. Phys.* **1991,** *74,* 1245–1263.
29. Kuchle, W.; Dolg, M.; Stoll, H.; Preuss, H. Energy-Adjusted Pseudopotentials for the Actinides. Parameter Sets and Test Calculations for Thorium and Thorium Monoxide. *J. Chem. Phys.* **1994,** *100,* 7535–7542.
30. Banisaukas, J.; Szczepanski, J.; Eyler, J. R.; Vala, M.; Hirata, S.; Head-Gordon, M.; Oomens, J.; Meijer, G.; von Helden, G. Vibrational and Electronic Spectroscopy of Acenaphthylene and Its Cation. *J. Phys. Chem. A* **2003,** *107,* 782–793.
31. Fielicke, A.; Mitric, R.; Meijer, G.; Bonacic-Koutecky, V.; von Helden, G. The Structures of Vanadium Oxide Cluster-Ethene Complexes. A Combined IR Multiple Photon Dissociation Spectroscopy and DFT Calculation Study. *J. Am. Chem. Soc.* **2003,** *125,* 15716–15717.
32. Foresman, J. B.; Frisch, A. E. *Exploring Chemistry with Electronic Structure Methods,* 2nd ed.; Gaussian: Pittsburgh, 1996.
33. Langhoff, S. R. Theoretical Infrared Spectra for Polycyclic Aromatic Hydrocarbon Neutrals Cations and Anions. *J. Phys. Chem.* **1996,** *100,* 2819–2841.
34. Cizek, J. Use of the Cluster Expansion and the Technique of Diagrams in Calculations of Correlation Effects in Atoms and Molecules. *Adv. Chem. Phys.* **1969,** *14,* 35–89.
35. Purvis, G. D. III.; Bartlett, R. J. A Full Coupled-Cluster Singles and Doubles Model: The Inclusion of Disconnected Triples. *J. Chem. Phys.* **1982,** *76,* 1910–1918.
36. Pople, J. A.; Head-Gordon, M.; Raghavachari, K. Quadratic Configuration Interaction. A General Technique for Determining Electron Correlation Energies. *J. Chem. Phys.* **1987,** *87,* 5968–5975.